RESEARCH PAPER

Flow of two immiscible liquids with low viscosity in Y shaped microfluidic systems: effect of geometry

Peiyuan He · Dominique Barthès-Biesel · Eric Leclerc

Abstract This article investigates the formation of albumin droplets in fatty esters by means of a flow focussing geometry where the continuous oil phase is introduced in the two lateral branches of a Y junction. The effect of the geometry is investigated in order to clarify the scales controlling the droplet generation with this type of fluid couple. The transition from regular droplet flow to stratified flow is identified from the experiments. It is found that the droplet size varies linearly with the flow rate ratio between the disperse and continuous phases. This is similar to what is found in T junctions microfluidic systems for low capillary numbers.

Keywords Two-phase flow · Droplet formation · Flow focussing · Thresholds of flow regimes

1 Introduction

The generation of monodisperse microdroplets is an important issue in many industrial domains and there are thus various techniques to produce such particles. They include for example, creating an emulsion by stirring the disperse phase into the continuous phase or pushing the disperse phase through a microporous membrane. However, these techniques all result in a fairly wide size distribution of the droplet population (Geerken et al. 2008). In some applications such as drug delivery or food engineering (Mc Clement et al. 2007), the formation of microdroplets is the first step for the preparation of microcapsules. The droplet size dispersion then leads to a dispersion in the capsule size and physical properties (e.g., membrane thickness) that can impair proper functioning of the capsules.

Recently, microfluidic devices have been investigated to prepare monodispersed microdroplets and microcapsules. The advantage of these devices lies in the possibility to produce micron size droplets in a confined geometry where the size of the microdroplets is controlled by the dimensions of the microchannels and by the flow rates of the dispersed and continuous phases. Some devices use a T junction geometry and different fluids phases such as oil/water (Thorsen et al. 2001; Anna et al. 2003), air–liquid (Stride et al. 2008) or liquid–liquid couples (Li et al. 2008). Models of the flow in a T junction have been proposed to predict the droplet formation (Stone et al. 2004; Garstecki et al. 2006; van der Graaf et al. 2006; Christopher and Anna 2007; Steegmans et al. 2009). In a second type of geometry, the droplets are created by injecting a central jet of liquid in another flowing liquid. In co-axial cylindrical jets, the mechanism of droplet formation is modeled by the Rayleigh Plateau theory (Guillot et al. 2007). However due to the microfabrication constraints, most of the flow focusing microfluidic devices consist of microchannels with square or rectangular sections rather than circular ones and the Rayleigh Plateau theory cannot be used to model microdroplet formation. The planar flow focusing microfluidic devices use either parallel or cross flows. Downstream of the junction, the inner fluid is

P. He · D. Barthès-Biesel (✉) · E. Leclerc (✉)
UMR CNRS 6600, Biomécanique et Bioingénierie, Université
de Technologie de Compiègne, Compiègne Cedex, France
e-mail: dbb@utc.fr

E. Leclerc
e-mail: eric.leclerc@utc.fr

P. He
e-mail: peiyuan.he@utc.fr

submitted to the pressure and shear stress exerted by the outer fluid, and to interfacial tension. When those forces are balanced, the situation is unstable and a droplet breaks off. The droplet size is again controlled by the intersection geometry and by the flow rates of the inner and outer fluids (Christopher and Anna 2007; Lee et al. 2009).

The studies of droplet formation in microfluidic devices are mostly performed with model fluids such as oil (or air) and water with the objective of investigating the micro-scale physics of droplet generation. The model fluids have a large contrast in physicochemical properties such as viscosity or interfacial tension that facilitates droplet formation. However, in cosmetic or pharmaceutical applications the emulsions often consist of an aqueous protein solution dispersed in a fatty ester such as ethylhexyl 2-ethylhexanoate (Hurteaux et al. 2005), methyl laurate (Bouchemal et al. 2004), isopropyl myristate (Kogan and Garti 2006; Subramanian et al. 2005) or isopropyl palmitate (Kogan and Garti 2006). Such emulsions are then commonly used to produce microcapsules. The surface tension is small and the viscosity ratio between the two phases is of order unity. This makes microdroplet formation more difficult than for classical oil/water couples. To our knowledge, there has been no study of the formation of microdroplets in microfluidic devices for two immiscible liquid phases with low viscosity contrast and low surface tension as is the case in pharmaceutical formulations. It is thus the objective of this article to investigate the formation of albumin micro droplets in fatty esters by means of a microfluidic device. We have selected a Y junction flow focussing geometry, where the protein solution is injected in a central jet and the fatty esters are injected laterally through the two branches of the Y. This geometry has the advantage of keeping the protein solution centered in the channel downstream of the junction and of preventing protein adsorption on the channel wall (Boxshall et al. 2006), contrarily to T junctions geometries where the injected flow is squeezed near a wall before breaking. We investigate the conditions for droplet generation with this type of fluid couple in different channel geometries in order to clarify the governing parameters and scales controlling the process. We find that, depending on the central to lateral flow rate ratio, droplets are formed regularly (dripping regime) or a stratified flow situation prevails with a steady central albumin solution thread surrounded by the oil phase.

We first present the experimental set-up and procedures in Sect. 2. We discuss the different flow regimes and investigate the conditions for transition from stratified flow to dripping flow in Sect. 3.3. The drop size is then analysed as a function of geometry and flow conditions in Sect. 3.4. The results are discussed and compared to those obtained in a T junction in the last section.

2 Materials and methods

2.1 Fluid phases

The disperse phase consists of a 20% solution of Human serum albumin (HSA) in a pH 9.8 phosphate buffer, with dynamic viscosity $\mu = 3.3$ mPa s at 25°C. The continuous phase is a biocompatible fatty ester. In most experiments, we used Dragoxat (2-ethylhexyl 2-ethylhexanoate, Symrise) with dynamic viscosity $\mu = 3.6$ mPa s at 25°C (Viscometer,Thermo Haake) and surface tension with HSA $\gamma = 0.006$ N/m (tensiometer Kruss DSA10 Mk2). For comparison purposes, we have also run a few experiments using methyl laurate, with $\mu = 5.5$ mPa s at 25°C and $\gamma = 0.0093$ N/m. It should be noted that albumin molecules tend to adsorb at the interface with the oil phase. A HSA-dodecane interface is saturated for a bulk HSA concentration of 10% (Chen et al. 1996). We can then expect the interface to be fully saturated (thus the low surface tension) so that Marangoni effects should not affect the drop formation process.

2.2 Micro-channels and experimental set-up

Polydimethylsiloxane (PDMS, Sylgard 184) microchannels are manufactured following a standard procedure (McDonald and Whitesides 2002). The mould master is made with a SU-8 photoresist material on a silicon wafer. The PDMS is poured, baked, peeled off the master and bound to a glass plate by air plasma. Four holes are drilled at the inlet and outlet of the microchannels for fluid perfusion or collection. As shown in Fig. 1, the microchip consists of a central channel (width W_c) intersected at an angle α by two identical lateral channels (width W_l). All channels of one system have a common depth h and a length of order 2 to 3 cm. The central channel ends in a reservoir with a gradual expansion, where the droplets are collected. The four parameters (W_c, α, W_l, h) determine the
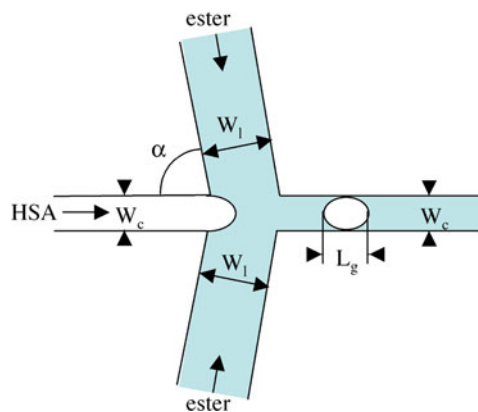

Fig. 1 Schematics of the micro-channel

Table 1 Geometrical parameters of the different systems, and corresponding symbol used in graphs

System	W_c (μm)	W_l (μm)	α (°)	h (μm)	W_c/h	W_c/W_l	Symbols
1	100	200	80	100	1	0.5	□
2	100	200	80	50	2	0.5	○
3	170	170	60	80	2.125	1	Δ

geometry of the Y junction microchip. The depth of the channel is equal to the master mould height which is measured by means of a surface profiler (Alpha Step IQ, TLA-Tencor). The width and depth of the microchannels are also checked by means of scanning electron microscope pictures. Three different geometries have been used where the ratios W_c/W_l and W_c/h are varied. The geometrical properties of the microchannels are summarized in Table 1.

2.3 Experimental procedure

The solutions are conserved at 4°C and heated to the room temperature of 25°C before use. The ester is introduced into the two lateral microchannels by means of a two-syringe pump (Bioblock, Illkirch, France) producing equal flow rates in each branch. The system is first flooded with Dragoxat. Then the HSA solution is introduced into the upper part of the central microchannel by means of another syringe pump. The flow rates in the central and in each lateral microchannel, respectively Q_c and Q_l, can thus be adjusted independently and can be varied between 2 and 120 μl/min, corresponding to velocities ranging between 3 and 180 mm/s in a 100×100 μm^2 channel. The droplets, if any, are then formed at the junction and convected in the downstream part C_{down} of the central channel. Flow visualisation at the junction is done by means of a high speed CDD camera (IF-865S) mounted on a conventional optical inverted microscope and connected to a computer (Matrox METEOR2-MC2 acquisition card). Data images are

recorded with a resolution corresponding to 100 pixels per 250 μm. Image size was 350×344 pixels respectively in width × height. 750 images are recorded at a frequency of 150 images/s. The experiments are repeated at least three times (or more) using new micro-systems each time.

3 Results

All the experiments have been done with Dragoxat as the continuous phase, except in Sect. 3.5, where laurate is used in order to assess the effect of the ester physical properties. The experimental procedure consists in setting the value of Q_l and then increasing Q_c progressively.

3.1 Flow regimes

We observe three different flow regimes for increasing values of Q_c, as reported repeatedly for different systems independent of the junction geometry (Anna et al. 2003; Husny and Cooper White 2008). For low values of Q_c, there is an initial transient regime where the central microchannel is invaded by the Dragoxat while the HSA jet is squeezed. This situation is obviously unstable and small slugs of HSA are ejected periodically. This cannot be assimilated to droplet formation as the process is not quite repeatable and depends on the mechanical characteristics of the perfusion pumps and the compliance of the system. This regime persists until a threshold is reached that is a function of the pressure drop in the channels, and thus of the flow rate ratio and channel geometry. In our systems, we find that this threshold is of order $Q_c/Q_l = 0.1$ in systems 1 and 3 and of order 0.2 in system 2 where the pressure drop is larger for the same value of flow rate.

When this low threshold is exceeded, we reach a steady dripping regime where droplets are formed regularly at the channel junction as shown in Fig. 2. As the HSA jet

Fig. 2 Successive phases of drop formation **a** in system 2, $Q_c/Q_l = 0.3$; **b** in system 3 $Q_c/Q_l = 0.6$
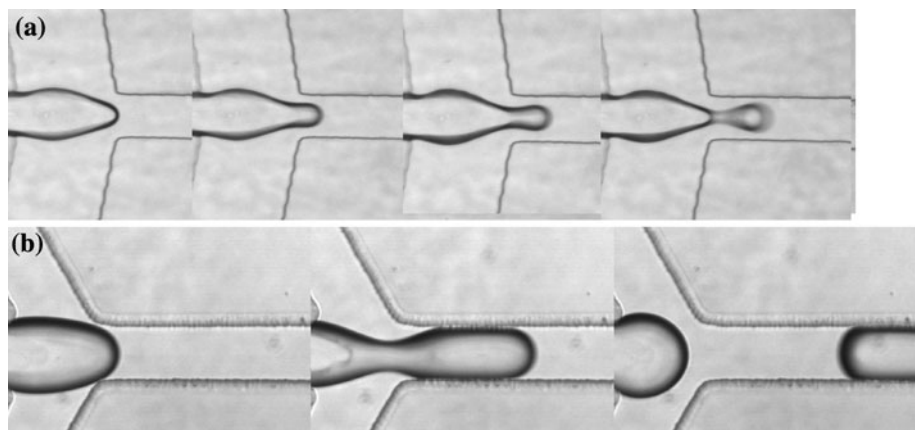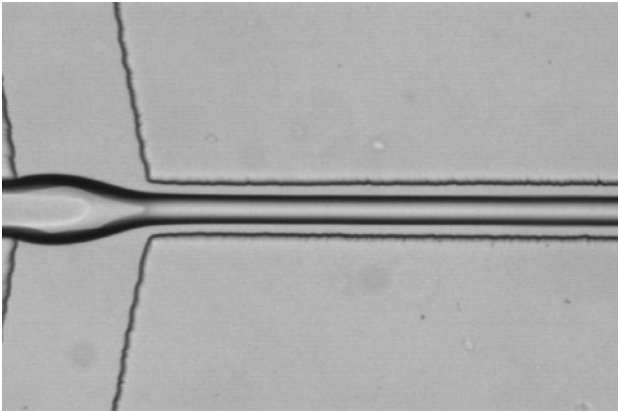
Fig. 3 Steady stratified flow with a central HSA liquid thread, $Q_c/Q_l = 0.94$, System 1

reaches the junction, it is stretched by the Dragoxat flow and enters the downstream part of the central channel. Then capillary forces break the HSA jet and a droplet is formed. When Q_c increases, the relative droplet size increases, as will be discussed in detail in the next section. The dripping regime persists until a higher limit is reached $[Q_l, Q_c]_{high}$ past which the HSA jet flows inside C_{down} without breaking and a steady stratified two phase flow is observed as shown in Fig. 3. The confined geometry of the channel inhibits the the development of a capillary instability as studied in detail in (Humphry et al. 2009).

The transition between the different regimes is difficult to get with precision. The reported values of $[Q_l, Q_c]_{high}$ are defined as the first value of Q_c (Q_l being fixed) for which the steady stratified flow is observed.

3.2 Stratified flow

When the threshold $[Q_l, Q_c]_{high}$ is exceeded, a steady central liquid thread of HSA is formed (Fig. 3) that is stable over the length of C_{down}. The width L_a of the thread depends on the channel geometry and on the values of Q_c/Q_l as shown in Fig. 5. The uniform axial velocity

distribution $u(y, z)$ in a rectangular duct can be found in a number of textbooks (see for example, Tabeling 2005):

$$u(y,z) = \frac{4h^2 G}{\pi^3 \mu} \sum_n \left[\frac{1}{n^3} - \frac{\cosh n\pi y/h}{n^3 \cosh n\pi W_c/2h} \right] \sin n\pi(z/h + 1/2),$$
$$n = 1, 3, \ldots \tag{1}$$

where G is the pressure gradient, and y and z the coordinates in a channel section (Fig. 4a). Since the two liquid viscosities are almost equal and surface tension is low, we assume that the axial velocity distribution $u(y, z)$ in the duct is given by Eq. 1. We further assume that the HSA liquid thread is centred in the duct and has an elliptical cross section S with the same aspect ratio as the duct and thus with semi diameters L_a and $H = L_a h/W_c$, (Fig. 4a). The flow rate of HSA is thus given by

$$Q_c = \int \int_S u(y, z) \mathrm{d}y \mathrm{d}z. \tag{2}$$

The inner integration over z is easily performed

$$Q_c = \frac{-16h^3 G}{\pi^4 \mu} \int_0^{L_a/2} \sum_n \frac{1}{n^4} \left[1 - \frac{\cosh n\pi y/h}{\cosh n\pi W_c/2h} \right]$$
$$\times \cos \left[n\pi \left(\frac{H}{h} \sqrt{1 - y^2/L_a^2} + 1/2 \right) \right] \mathrm{d}y, \tag{3}$$

The total flow rate $Q_t = Q_c + 2Q_l$ in the channel is given by

$$Q_t = 4 \int_0^{W_c/2} \int_0^{h/2} u(y, z) \mathrm{d}y \mathrm{d}z \tag{4}$$

$$Q_t = \frac{8h^3 G W_c}{\pi^4 \mu} \left[\frac{\pi^4}{96} - \sum_n \frac{\tanh n\pi W_c/2h}{n^5 \pi W_c/2h} \right] \quad n = 1, 3, \ldots \tag{5}$$

The numerical integration of (3) leads to a non-linear relation between Q_c/Q_l and L_a/W_c as shown in Fig. 5. For duct aspect ratios W_c/h of order 2 or less, the relation between Q_c/Q_l and L_a/W_c does not depend much on the duct geometry. In the the range $0 < Q_c/Q_l < 2.5$, the

Fig. 4 Schematics of the flow in a channel cross section. The HSA central thread has width L_a and height $L_a h/W_c$
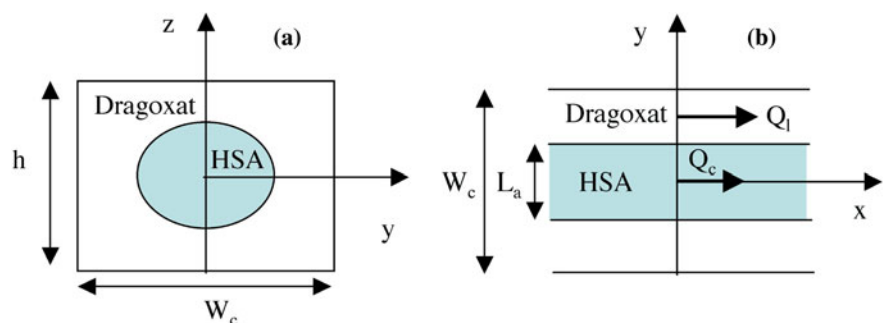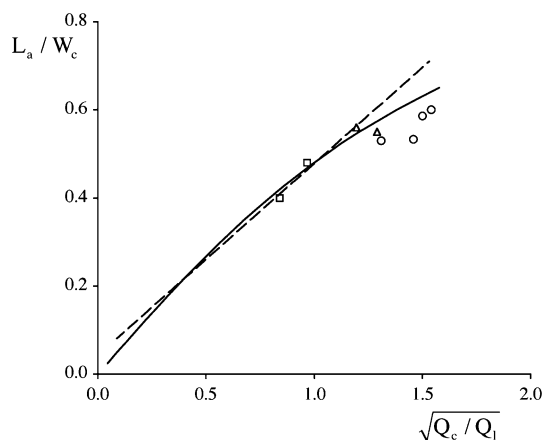
Fig. 5 Relation between the central jet width L_a/W_c and the flow rate ratio Q_c/Q_l for ducts with aspect ratio $1 \leq h/W_c < 2.2$. *Full line*: exact solution; *dashed line*: linear correlation (6); *symbols* (defined in Table 1): experimental data in systems 1, 2, 3

relation between central jet width and flow rate ratio can be approximated by

$$L_a/W_c \approx 0.4\sqrt{Q_c/Q_l} + 0.05, \quad R^2 = 0.98. \tag{6}$$

As shown in Fig. 5, the experimental measures of central thread width in Systems 1 and 3 correlate very well with either the exact solution or the approximate relation (6). The measurements for system 2 fall a little below the exact solution (by 6% at most). This may be due to the fact that in a rectangular duct with $W_c/h = 2$, the hypothesis of an elliptical central thread is not quite accurate.

3.3 Transition from dripping to laminar flow

The transition from regular droplet flow to laminar flow depends on the geometry of the junction and of the the channels as well as on the flow dynamics, but we can make an order-of-magnitude estimate. We first note that the flow Reynolds number varies between 0.1 and 6, the highest value corresponding to a central flow rate $Q_c = 120$ μl/min. This means that inertia effects are not very important can be neglected in a first approach. Consider the laminar flow in half the central channel (Fig. 4b). The HSA and Drag-oxat film thicknesses are $L_a/2$ and $(W_c - L_a)/2$, respectively, with corresponding mean velocities u_c and u_l. When a drop is forming, the surface tension stress is of order $\sigma_{cap} = \gamma(2/h + 2/W_c)$, where γ is the surface tension between the two phases and where we have assumed a longitudinal disturbance of order W_c for the laminar jet. The viscous stress exerted by the external flow is of order $\sigma_{visc} = 2\mu u_l/(W_c - L_a)$ with $u_l = 2Q_l/h(W_c - L_a)$. We assume that droplets are formed when the capillary forces exceed viscous effects. This condition can be expressed in terms of a critical capillary number Ca:

$$\frac{\sigma_{visc}}{\sigma_{cap}} \leq Ca$$

Replacing the stresses by their order of magnitude, we find

$$Q_l \leq \frac{\gamma Ca}{2\mu}(1 + h/W_c)W_c^2(1 - L_a/W_c)^2. \tag{7}$$

Keeping in mind that L_a/W_c is smaller than unity and usually less than 0.5 in our experiments, we neglect quadratic terms and the constant term in (6)

$$Q_l \leq A(1 - 2L_a/W_c). \tag{8}$$

The constant A has the dimensions of a flow rate and is given by

$$A = \frac{\gamma Ca}{2\mu}(1 + h/W_c)W_c^2. \tag{9}$$

Finally, using the laminar flow correlation for the central jet width (6), we obtain the condition for droplet formation

$$Q_c \leq 1.6(Q_l - 2Q_l^2/A + Q_l^3/A^2), \tag{10}$$

As explained earlier, we have defined $[Q_l, Q_c]_{high}$ as the first couple of flow rate values for which a steady central thread of HSA occurred in C_{down}. The experimental limiting values of Q_c and Q_l are shown in Fig. 6 together with a quadratic fit of each data set. We find, respectively,

$$Q_c = -0.0084Q_l^2 + 1.9Q_l - 18, \quad R^2 = 0.967 \\ \text{for system 1,} \tag{11}$$

$$Q_c = -0.012Q_l^2 + 2.6Q_l - 21, \quad R^2 = 0.993 \\ \text{for system 2,} \tag{12}$$

where the flow rates are expressed in μl/min. The coefficients of the Q_l^2 term give us the values of A for both systems. We find $A_1 = 381$ μl/min for system 1 and $A_2 = 266$ μl/min for system 2. The term Q_l^3/A^2 is negligible in (10), because A is much larger than the

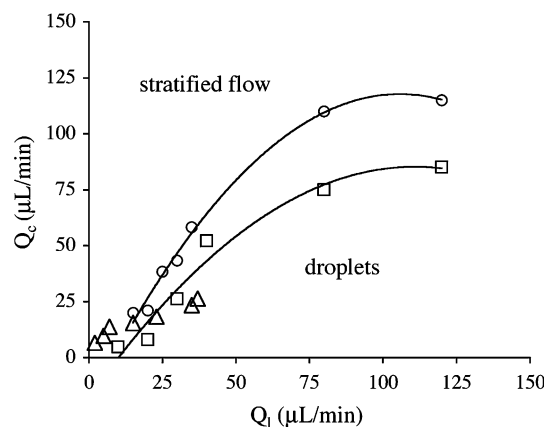**Fig. 6** High threshold values of Q_c and Q_l (in μl/min) where transition occurs from dripping to jetting. The system symbols are given in Table 1. The *full lines* represent quadratic fits

experimental flow rates we used. The experimental value of the ratio $A_1/A_2 = 1.45$ is very near the one that can be estimated from (10), namely $(1 + h_1/W_{c1})/(1 + h_2/W_{c2}) = 1.33$. The critical capillary number for which a droplet forms is found to be Ca ≈ 0.3, a value which is of the same order of magnitude that what is obtained for the breakup of liquid droplets freely suspended in an unbounded shear flow (Stone 1994). Note too, that the linear term in correlations (11) and (12) has a coefficient of order 2 when the analysis predicts a value of 1.6. Considering the difficulty of threshold detection and the approximations made in the transition analysis, the agreement can be considered as quite good. This means that the proper physical phenomenon has been accounted for.

3.4 Droplet flow

When droplets form regularly, the different phases of the process are depicted in Fig. 2a, b. There are two slightly different drop formation processes that depend on the size of the intersection. For a large intersection such that $W_1 > W_c$, the HSA jet occupies the centre of the intersection as depicted in Fig. 2a. The tip of the jet extends under the effect of the continuous flow of HSA and of the Dragoxat elongational flow. The tip of the HSA jet enters the downstream channel, the elongational effect of the Dragoxat increases and the jet is broken, thus forming a droplet. For smaller intersections such that $W_1 = W_c$, the process is different as shown in Fig. 2b. There is no steady HSA jet in the intersection, but the jet emerges from C_{up} every time a droplet is formed. The jet then enters quickly C_{down} and is broken in a fashion similar to that of the previous case.

We measure the length L_g of the droplet flowing down C_{down}. If the droplet moves too fast for the camera exposure time, it is blurred. In order to limit this phenomenon, we have used flow rates Q_c and Q_1 in the range of 2–40 µl/min, corresponding to a maximum velocity of 60 mm/s in a 100×100 µm^2 channel. The droplet length is measured with a precision of ±10 µm. The results presented in this section have been repeated with different systems fabricated from the same mould. The dispersion is due to small experimental errors in the pump setting, system compliance and the non linear dynamics of the dripping regime. For a given value of Q_1, the droplet length increases with Q_c, but for a given value of Q_c, the droplet length decreases with Q_1. This is in accordance with the experimental or numerical results obtained in T or planar flow-focussing geometries (Stone et al. 2004; Garstecki et al. 2006; Husny and Cooper White 2008; van der Graaf et al. 2006; Lee et al. 2009). For the range of tested values, the drop length normalized with the channel height increases linearly with the flow rate ratio Q_c/Q_1, provided it is larger than the lower limit mentioned in section 3.1 (Fig. 7). This result is qualitatively consistent
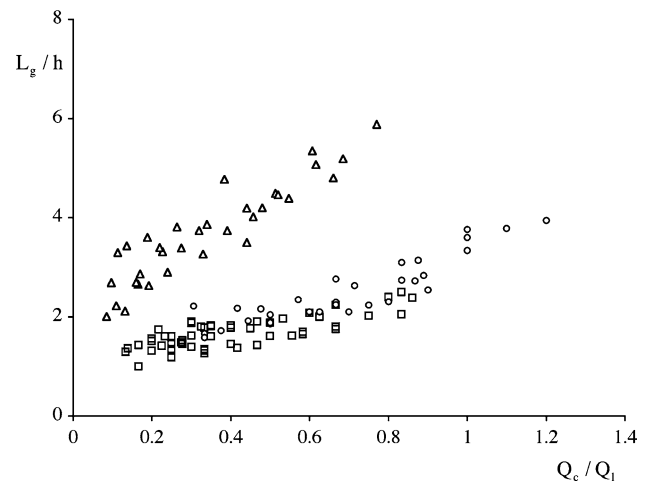

Fig. 7 Normalized drop length L_g/h as a function of flow rate ratio Q_c/Q_1 for HSA droplet in Dragoxat. Results for systems 1 (*open square*) and 2 (*open circle*) are superimposed although their heights h are in the ratio 2:1. System 3 (*open triangle*) has an intermediate height but a different intersection geometry

with data reported in a T junction at low Capillary number (Stone et al. 2004). However, we find a significant effect of geometry. For example, it is interesting to note that the values obtained for systems 1 and 2 are nearly superimposed when L_g is normalised with the system heights h that are in the ratio 2:1. The values obtained for system 3 with an intermediate height but a different intersection geometry are significantly higher. This shows that the geometry of the junction plays an important role.

The dripping hydrodynamic regime is unsteady, and the flow rates at the junction fluctuate with time. This dynamic process is very complicated as it involves the interplay of viscous and capillary forces. To our knowledge, there is no simple model of the two-phase flow in a Y junction, that can predict the dimensions of the droplets as a function of the system parameters such as geometry, flow rates and fluid physical properties. It is possible, however, to analyze the physics of the system and estimate how the droplet size should vary. The droplet volume V_g is equal to $Q_c\tau$, where τ is the time of formation of a drop. Following Stone and co-workers (Stone et al. 2004; Garstecki et al. 2006), we estimate τ to be the time the external liquid takes to squeeze the HSA jet. It is proportional to W_c/u_1 where u_1 is the velocity of the external liquid near the entrance to C_{down}. The exact value of u_1 is not available as it depends on the two fluid configuration in the intersection, but it is proportional to the velocity $Q_1/(h W_1)$ in a lateral channel. Consequently, we can expect the drop volume to be given by

$$V_g = L_g W_c h = KQ_c\tau = KQ_c\frac{W_c}{Q_1/(hW_1)}, \qquad (13)$$

where K is a numerical constant that depends on the system geometry and physical properties such as viscosity contrast
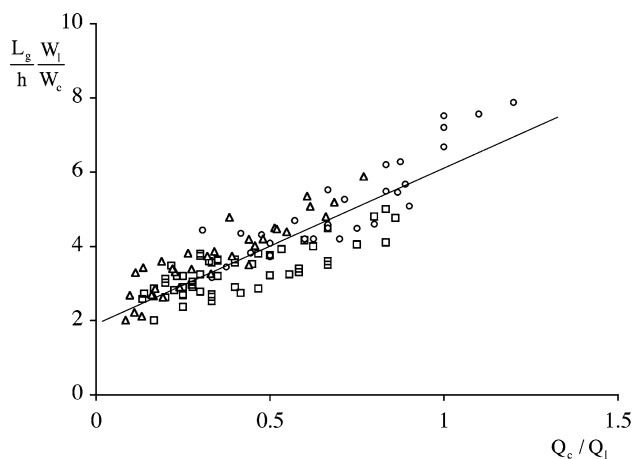
Fig. 8 Drop length L_g renormalized with hW_c/W_l as a function of flow rate ratio Q_c/Q_l for HSA droplet in Dragoxat. The symbols refer to the different systems as defined in Table 1. All data points fall approximately on the same linear correlation

and capillary number. The droplet length is thus a linear function of the flow rate ratio as is indeed the case (Fig. 7). If we renormalize all the experimental drop lengths of Fig. 7 to account for the intersection geometry measured by W_c/W_l, we find that the results for the three systems fall approximately on the same line, as shown in Fig. 8. Consequently, from this experimental correlation, we find that for the HSA/Dragoxat fluid couple, the slug length is given by

$$L_g/h = 4.1 \frac{W_c}{W_l}\frac{Q_c}{Q_l} + 1.9 \frac{W_c}{W_l}. \qquad (14)$$

This correlation is valid for flow rate ratios between 0.1 and 1–1.4. Higher values of Q_c/Q_l leads to stratified flow situations as discussed in Sect. 3.2.

3.5 Effect of the continuous phase properties

In order to assess the effect of the fluids physical properties, we now replace Dragoxat with methyl laurate, another fatty acid also commonly used in pharmaceutical industry. The disperse phase is the same HSA solution. The continuous phase has now a viscosity that is 1.5 that of the disperse phase. We then study droplet size as a function of flow rates in systems 1, 2 and 3, but do not try to identify the high threshold for stratified flow. As shown in Fig. 9, we find again that L_g/h varies linearly with Q_c/Q_l and that the results for systems 1 and 2 are superimposed. The correlation giving droplet length as a function of flow rate ratio and geometry is now

$$L_g/h = 2.5 \frac{W_c}{W_l}\frac{Q_c}{Q_l} + 1.5 \frac{W_c}{W_l}. \qquad (15)$$

We obtain a correlation that is different from (14) because the viscosity ratio between the continuous and disperse phase is now 1.5 instead of 1.
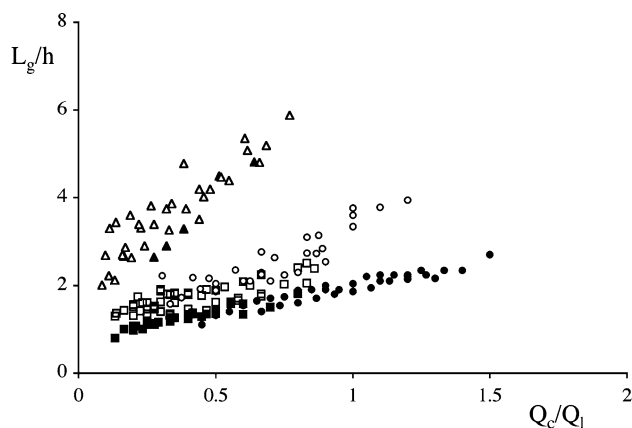

Fig. 9 Drop length as a function of flow rate ratio in the three systems (symbols defined in Table 1) for two continuous phases with different viscosity. *Open symbols*: Dragoxat, *filled symbols*: laurate. The same linear trend is observed for the more viscous continuous phase, laurate
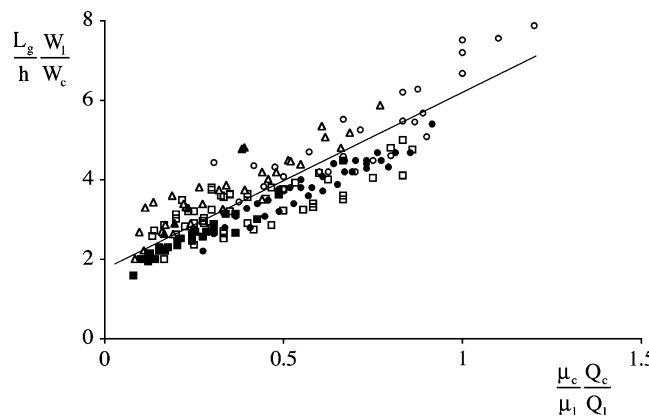

Fig. 10 Drop length L_g renormalized with hW_c/W_l as a function of ratio $\mu_c Q_c/\mu_l Q_l$ for HSA droplet in Dragoxat or laurate. The symbols refer to the different systems as defined in Table 1, *open symbols*: dragoxat, *filled symbols*: laurate. All data points fall approximately on the same linear correlation

However, if we plot the drop length as a function of the viscous stress ratio, measured by $\mu_c Q_c/\mu_l Q_l$, we find that the results from the Dragoxat and laurate superimpose as shown in Fig. 10. From this study, we may conclude that in the Y junction that we studied and for the HSA/fatty esters systems, the drop length is given by

$$L_g/h = 4.1 \frac{Q_c}{Q_l}\frac{\mu_c}{\mu_l}\frac{W_c}{W_l} + 1.8 \frac{W_c}{W_l} \quad R^2 = 0.81. \qquad (16)$$

This relation is useful for controlling the droplet volume as a function of flow rate, system geometry and fluid properties.

4 Discussion and conclusion

We have studied the formation of droplets for a specific two fluid system with low viscosity contrast in a geometry

that differs from the classical T junction or planar flow focussing. The Y junction has been designed to avoid albumin adsorption on the PDMS walls. Furthermore, as we first fill the system with the oil phase and then inject the HSA solution, we assume that the oil coats the channel walls of the junction and of C_{down}, and thus that the droplets are fully detached from the wall. We have also assumed that the droplets were centred in the channel due to lubrication forces. The drawback with using a Y junction is that there are yet no systematic studies of drop formation in this geometry like those one can find for T junctions or planar flow focussing systems.

Droplet formation of water in oil, inside microfluidic channels, has been extensively described in T shape microchannels (see the review Steegmans et al. 2009). In particular, Garstecki et al. (2006) found that the characteristic length of the droplet was proportional to flow rate ratio $L_g/W_c = 1 + \beta Q_c/Q_l$ (in terms of our notations), where β is a parameter of order 1. This relation has been obtained when the external flow capillary number $Ca_l = \mu_l u_l/\gamma$ was very small ($Ca_l \sim 0.01$). For higher values $Ca_l \geq 1$, the droplet length was reported to be a non linear function of Q_c/Q_l (Adzima and Velankar 2006; Xu et al. 2006). In our case, the capillary number in each lateral channel is $Ca_l \sim 0.01-0.1$. This may explain why the correlation (16) is linear and similar to the one of Garstecki et al. If we normalise the drop length with the channel width rather than the depth, we find

$$L_g/W_c = 4.1\frac{Q_c}{Q_l}\frac{\mu_c}{\mu_l}\frac{h}{W_l} + 1.8\frac{h}{W_l}, \quad \text{for} \quad \frac{Q_c}{Q_l} > 0.1, \quad (17)$$

which shows how β depends on the channel geometry and fluid properties. It should be noted that the droplet size is determined by the smallest dimension (here, the depth) of the injection channel and that it is not possible to product droplets with a length smaller than h in this regime. This correlation is of course valid for a fluid system with a O(1) viscosity ratio in cross flow systems with geometrical properties in the range of those tested here, namely $W_c/h \in [1, 2]$ and $W_l/W_c \in [1, 2]$. For example, we have been unable to create droplets in channels with $W_c/h \geq 4$ using the full range of flow rates.

We cannot assess the effect of Ca_l in an unambiguous fashion with the two different fluid systems we used. One reason is that we do not have a wide enough range of values of Q_l for a given Q_c because we hit the high threshold rather quickly. We have used two different liquid phases with different viscosity and surface tension. However, for a given lateral flow velocity u_l, we obtain the same value of capillary number for Dragoxat and laurate because the ratio μ/γ has almost the same value for the two liquid systems. Finally, for a system with a small viscosity

contrast, it could well be that the inner capillary number plays an equally important role as the outer capillary number.

In conclusion, we find that a Y junction flow focussing microfluidic device allows to create droplets through a process that is similar to the one that occurs in T junction for low capillary numbers. In Y junction systems, droplet creation does not necessitate large lateral flow rates and can be achieved for flow rate ratios Q_c/Q_l of order unity or less. Another advantage is that the lateral fluid is brought in contact with the disperse phase in a symmetrical way. In the case where reagents are carried in the continuous phase, this may be beneficial as it leads to a better distribution of chemicals on the surface of the droplet.

References

Adzima B, Velankar S (2006) Pressure drop for droplet flows in microfluidic channels. J Micromech Microeng 16:1504–1510

Anna S, Bontoux N, Stone HA (2003) Formation of dispersions using "flow focusing" in microchannels. Appl Phys Lett 82:364–366

Bouchemal K, Briancon S, Perrier E, Fessi H (2004) Nano-emulsion formulation using spontaneous emulsification: solvent, oil and surfactant optimisation. Int J Pharm 280:241–251

Boxshall K, Wu M-H, Cui Z, Cui Z, Watts JF, Baker MA (2006) Simple surface treatments to modify protein adsorption and cell attachment properties within a poly(dimethylsiloxane) micro-bioreactor. Surf Interface Anal 38:198–201

Chen P, Lahooti S, Policova Z, Cabrerizo-Vilchez MA, Neumann AW (1996) Concentration dependance of the film pressure of human serum albumin at the water/decane interface. Colloids Surf B 6:279–289

Christopher GF, Anna SL (2007) Microfluidic methods for generating continuous droplet streams. J Phys D 40:R319–R336

Garstecki P, Fuerstman MJ, Stone H, Whitesides G (2006) Formation of droplets and bubbles in a microfluidic t-junction-scaling and mechanism of break up. Lab on a Chip 6:437–446

Geerken M, Groenendijk M, Lammertink R, Wessling M (2008) Micro-fabricated metal nozzle plates used for water-in-oil and oil-in-water emulsification. J Membr Sci 310:374–383

Guillot P, Colin A, Utada AS, Ajdari A (2007) Stability of a jet in confined pressure-driven biphasic flows at low Reynolds number. Phys Rev Lett 99:104502–104504

Humphry KJ, Ajdari A, Fernandez-Nieves A, Stone HA, Weitz DA (2009) Suppression of instabilities in multiphase flow by geometric confinement. Phys Rev E 79:056310

Hurteaux R, Edwards-Levy F, Laurent-Maquin D, Levy MC (2005) Coating alginate microspheres with a serum albumin-alginate

membrane: application to the encapsulation of a peptide. Eur J Pharm Sci 24:187–197

Husny J, Cooper White J (2006) The effect of elasticity on drop creation in t-shaped microchannels. J Non-Newtonian Fluid Mech 137:121–136

Kogan A, Garti N (2006) Microemulsions as transdermal drug delivery vehicles. Adv Colloid Interface Sci 123-126:369–385

Lee W, Walker LM, Anna SL (2009) Role of geometry and fluid properties in droplet and thread formation processes in planar flow focussing. Phys Fluids 21:032103

Li S, Xu J, Wang Y, Luo G (2008) Controllable preparation of nanoparticles by drops and plugs flow in a microchannel device. Langmuir 24:4194–4199

Mc Clement DJ, Decker EA, Weiss J (2007) Emulsion-based delivery systems for lipophilic bioactive components. J Food Sci 72:R109–R124

McDonald JC, Whitesides GM (2002) Poly(dimethylsiloxane) as a material for fabricating microfluidic devices. Acc Chem Res 35:491–499

Steegmans MLJ, Schroen CGPH, Boom RM (2009) Generalized insights in droplet formation at t-junctions through statistical analysis. Chem Eng Sc 64:3042–3050

Stone HA, Stroock AD, Ajdari A (2004) Engineering flows in small devices: Microfluidics towards a lab-on-a-chip. Lab on a Chip 36:381–412

Stone HA (1994) Dynamics of drop deformation and breakup in viscous fluids. Ann Rev Fluid Mech 26:65–102

Stride E, Pancholi K, Edirisinghe M (2008) Dynamics of bubble formation in highly viscous liquids. Langmuir 24:4388–4393

Subramanian N, Ghospal S, Acharya A, Moulik S (2005) Formulation and physicochemical characterization of microemulsion system using isopropyl myristate, medium-chain glyceride, polysorbate 80 and water. Chem Pharm Bull 53:1530–1535

Tabeling P (2005) Introduction to microfluidics. Oxford University Press, Oxford

Thorsen T, Roberts RW, Arnold FH, Quake SR (2001) Dynamic pattern formation in a vesicle-generating microfluidic device. Phys Rev Lett 86:4163–4166

van der Graaf S, Nisisako T, Schroen CGPH, van der Sman RGM, Boom RM (2006) Lattice boltzmann simulation of droplet formaation in a t-shpaed microchannel. Langmuir 22:4144–4152

Xu JH, Luo GS, Li SW, Chen GG (2006) Shear force induce monodisperse droplet formation in a microfluidic device by controlling wetting properties. Lab on a Chip 6:131